include TINAGL1, during blastocyst formation *in vitro* may affect subsequent postimplantation embryonic development.

Acknowledgements

This work was supported by the Japan Society for the Promotion of Science Grant to E. Sato (No. 21248032).

References

Armant, D.R., Kaplan, H.A. & Lennarz, W.J. (1986). Fibronectin and laminin promote *in vitro* attachment and outgrowth of mouse blastocysts. *Dev. Biol.* **116**, 519–23.

Aumailley, M. & Timpl, R. (1986). Attachment of cells to basement membrane collagen type IV. *J. Cell Biol.* **103**, 1569–75.

Bartlett, S.E. & Menino, A.R., Jr (1995). Evaluation of extracellular matrices and the plasminogen activator system in sheep inner cell mass and trophectodermal outgrowth *in vitro*. *Biol. Reprod.* **52**, 1436–45.

Burrows, T.D., King, A. & Loke, Y.W. (1993). Expression of integrins by human trophoblast and differential adhesion to laminin or fibronectin. *Hum. Reprod.* (Oxford, England) **8**, 475–84.

Carnegie, J.A. (1991). Immunolocalization of fibronectin and laminin within rat blastocysts cultured under serum-free conditions. *J. Reprod. Fertil.* **91**, 423–34.

Carnegie, J.A. & Cabaca, O. (1991). The influence of extracellular matrix components on the proliferation and migration of inner cell mass-derived parietal endodermal cells. *Biol. Reprod.* **45**, 572–80.

Carnegie, J.A. & Cabaca, O. (1993). Extracellular matrix composition and resilience: two parameters that influence the *in vitro* migration and morphology of rat inner cell mass-derived cells. *Biol. Reprod.* **48**, 287–99.

Damsky, C.H., Librach, C., Lim, K.H., Fitzgerald, M.L., McMaster, M.T., Janatpour, M., Zhou, Y., Logan, S.K. & Fisher, S.J. (1994). Integrin switching regulates normal trophoblast invasion. *Development* (Cambridge, England) **120**, 3657–66.

Dey, S.K., Lim, H., Das, S.K., Reese, J., Paria, B.C., Daikoku, T. & Wang, H. (2004). Molecular cues to implantation. *Endocrine Rev.* **25**, 341–73.

Ecker, D.J., Stein, P., Xu, Z., Williams, C.J., Kopf, G.S., Bilker, W.B., Abel, T. & Schultz, R.M. (2004). Long-term effects of culture of preimplantation mouse embryos on behavior. *Proc. Natl. Acad. Sci. USA* **101**, 1595–600.

Fernandez-Gonzalez, R., Moreira, P., Bilbao, A., Jimenez, A., Perez-Crespo, M., Ramirez, M.A., Rodriguez De Fonseca, F., Pintado, B. & Gutierrez-Adan, A. (2004). Long-term effect of *in vitro* culture of mouse embryos with serum on mRNA expression of imprinting genes, development, and behavior. *Proc. Natl. Acad. Sci. USA* **101**, 5880–5.

Giritharan, G., Talbi, S., Donjacour, A., Di Sebastiano, F., Dobson, A.T. & Rinaudo, P.F. (2007). Effect of *in vitro* fertilization on gene expression and development of mouse preimplantation embryos. *Reproduction* (Cambridge, England), **134**, 63–72.

Hierck, B.P., Thorsteinsdottir, S., Niessen, C.M., Freund, E., Iperen, L.V., Feyen, A., Hogervorst, F., Poelmann, R.E., Mummery, C.L. & Sonnenberg, A. (1993). Variants of the alpha 6 beta 1 laminin receptor in early murine development: distribution, molecular cloning and chromosomal localization of the mouse integrin alpha 6 subunit. *Cell Adhes. Commun.* 1, 33–53.

Hoshino, Y. & Sato, E. (2008). Protein kinase B (PKB/Akt) is required for the completion of meiosis in mouse oocytes. *Dev. Biol.* **314**, 215–23.

Hynes, R.O. (1990). *Fibronectins*, New York: Springer-Verlag.

Igarashi, T., Tajiri, Y., Sakurai, M., Sato, E., Li, D., Mukai, K., Suematsu, M., Fukui, E., Yoshizawa, M. & Matsumoto, H. (2009). Tubulointerstitial nephritis antigen-like 1 is expressed in extraembryonic tissues and interacts with laminin 1 in the Reichert membrane at postimplantation in the mouse. *Biol. Reprod.* **81**, 948–55.

Irving, J.A., Lysiak, J.J., Graham, C.H., Hearn, S., Han, V.K. & Lala, P.K. (1995). Characteristics of trophoblast cells migrating from first trimester chorionic villus explants and propagated in culture. *Placenta* **16**, 413–33.

Laurie, G.W., Bing, J.T., Kleinman, H.K., Hassell, J.R., Aumailley, M., Martin, G.R. & Feldmann, R.J. (1986). Localization of binding sites for laminin, heparan sulfate proteoglycan and fibronectin on basement membrane (type IV) collagen. *J. Mol. Biol.* **189**, 205–216.

Leivo, I., Vaheri, A., Timpl, R. & Wartiovaara, J. (1980). Appearance and distribution of collagens and laminin in the early mouse embryo. *Dev. Biol.* **76**, 100–14.

Li, D., Mukai, K., Suzuki, T., Suzuki, R., Yamashita, S., Mitani, F. & Suematsu, M. (2007). Adrenocortical zonation factor 1 is a novel matricellular protein promoting integrin-mediated adhesion of adrenocortical and vascular smooth muscle cells. *FEBS J.* **274**, 2506–22.

Matsumoto, H., Ma, W., Smalley, W., Trzaskos, J., Breyer, R.M. & Dey, S.K. (2001). Diversification of cyclooxygenase-2-derived prostaglandins in ovulation and implantation. *Biol. Reprod.* **64**, 1557–65.

Matsumoto, H., Daikoku, T., Wang, H., Sato, E. & Dey, S.K. (2004). Differential expression of ezrin/radixin/moesin (ERM) and ERM-associated adhesion molecules in the blastocyst and uterus suggests their functions during implantation. *Biol. Reprod.* **70**, 729–36.

McRae, A.C. & Church, R.B. (1990). Cytoplasmic projections of trophectoderm distinguish implanting from preimplanting and implantation-delayed mouse blastocytes. *J. Reprod. Fertil.* **88**, 31–40.

Mohan, M., Hurst, A.G. & Malayer, J.R. (2004). Global gene expression analysis comparing bovine blastocysts flushed on day 7 or produced *in vitro*. *Mol. Reprod. Dev.* **68**, 288–98.

Mukai, K., Mitani, F., Nagasawa, H., Suzuki, R., Suzuki, T., Suematsu, M. & Ishimura, Y. (2003). An inverse correlation between expression of a preprocathepsin B-related protein with cysteine-rich sequences and steroid 11beta-hydroxylase in adrenocortical cells. *J. Biol. Chem.* **278**, 17084–92.

Murray, J.C., Stingl, G., Kleinman, H.K., Martin, G.R. & Katz, S.I. (1979). Epidermal cells adhere preferentially to type IV (basement membrane) collagen. *J. Cell Biol.* **80**, 197–202.

Nilsson, O. (1966). Structural differentiation of luminal membrane in rat uterus during normal and experimental

implantations. *Zeitschrift fur Anatomie und Entwicklungsgeschichte* **125**, 152–9.

Paria, B.C., Huet-Hudson, Y.M. & Dey, S.K. (1993). Blastocyst's state of activity determines the "window" of implantation in the receptive mouse uterus. *Proc. Natl. Acad. Sci. USA* **90**, 10159–62.

Paria, B.C., Ma, W., Tan, J., Raja, S., Das, S.K., Dey, S.K. & Hogan, B.L. (2001). Cellular and molecular responses of the uterus to embryo implantation can be elicited by locally applied growth factors. *Proc. Natl. Acad. Sci. USA* **98**, 1047–52.

Psychoyos, A. (1973). Endocrine control of egg implantation. In: *Handbook of Physiology* (Greep, R.O., Astwood, E.B. & Geiger, S.R., eds) American Physiological Society, Washington, DC, pp. 187–215.

Rinaudo, P. & Schultz, R.M. (2004). Effects of embryo culture on global pattern of gene expression in preimplantation mouse embryos. *Reproduction* **128**, 301–11.

Rinaudo, P.F., Giritharan, G., Talbi, S., Dobson, A.T. & Schultz, R.M. (2006). Effects of oxygen tension on gene expression in preimplantation mouse embryos. *Fertil. Steril.* **86**, 1252–65, 1265.e1–36.

Rubin, K., Hook, M., Obrink, B. & Timpl, R. (1981). Substrate adhesion of rat hepatocytes: mechanism of attachment to collagen substrates. *Cell* **24**, 463–70.

Salamat, M., Gotz, W., Werner, J. & Herken, R. (1993). Ultrastructural localization of lectin-binding sites in different basement membranes. Histochem. J. **25**, 464–8.

Schilperoort-Haun, K.R. & Menino, A.R., Jr. (2002a). Evaluation of extracellular matrix proteins and tissue inhibitor of matrix metalloproteinases-2 on bovine inner cell mass outgrowth *in vitro*. *In Vitro Cell. Dev. Biol.* **38**, 41–7.

Schilperoort-Haun, K.R. & Menino, A.R., Jr. (2002b). Factors affecting cellular outgrowth from porcine inner cell masses *in vitro*. *J. Anim. Sci.* **80**, 2671–80.

Sherman, M.I., Gay, R., Gay, S. & Miller, E.J. (1980). Association of collagen with preimplantation and peri-implantation mouse embryos. *Dev. Biol.* **74**, 470–8.

Stephens, L.E., Sutherland, A.E., Klimanskaya, I.V., Andrieux, A., Meneses, J., Pedersen, R.A. & Damsky, C.H. (1995). Deletion of beta 1 integrins in mice results in inner cell mass failure and peri-implantation lethality. *Genes Dev.* **9**, 1883–95.

Summers, M.C., McGinnis, L.K., Lawitts, J.A., Raffin, M. & Biggers, J.D. (2000). IVF of mouse ova in a simplex optimized medium supplemented with amino acids. *Hum. Reprod.* (Oxford, England), **15**, 1791–801.

Sutherland, A.E., Calarco, P.G. & Damsky, C.H. (1988). Expression and function of cell surface extracellular matrix receptors in mouse blastocyst attachment and outgrowth. *J. Cell Biol.* **106**, 1331–48.

Thorsteinsdottir, S. (1992). Basement membrane and fibronectin matrix are distinct entities in the developing mouse blastocyst. *Anat. Rec.* **232**, 141–9.

Wang, H. & Dey, S.K. (2006). Roadmap to embryo implantation: clues from mouse models. *Nat. Rev.* **7**, 185–99.

Wartiovaara, J., Leivo, I. & Vaheri, A. (1979). Expression of the cell surface-associated glycoprotein, fibronectin, in the early mouse embryo. *Dev. Biol.* **69**, 247–57.

Yelian, F.D., Yang, Y., Hirata, J.D., Schultz, J.F. & Armant, D.R. (1995). Molecular interactions between fibronectin and integrins during mouse blastocyst outgrowth. *Mol. Reprod. Dev.* **41**, 435–48.

Yohkaichiya, T., Hoshiai, H., Uehara, S. & Yajima, A. (1988). Fibronectin localization in the mouse embryo from the two cell stage to the morula stage. *Tohoku J. Exp. Med.* **154**, 95–100.

Yoshinaga, K. & Adams, C.E. (1966). Delayed implantation in the spayed, progesterone treated adult mouse. *J. Reprod. Fertil.* **12**, 593–5.

Zetter, B.R. & Martin, G.R. (1978). Expression of a high molecular weight cell surface glycoprotein (LETS protein) by preimplantation mouse embryos and teratocarcinoma stem cells. *Proc. Natl. Acad. Sci. USA* **75**, 2324–8.

Eukaryotic Cell

Outer Dynein Arm Light Chain 1 Is Essential for Controlling the Ciliary Response to Cyclic AMP in Paramecium tetraurelia

Osamu Kutomi, Manabu Hori, Masaki Ishida, Takashi Tominaga, Hiroyuki Kamachi, France Koll, Jean Cohen, Norico Yamada and Munenori Noguchi

Eukaryotic Cell **2012, 11(5):645. DOI: 10.1128/EC.05279-11. Published Ahead of Print 16 March 2012.**

EC
Journals.ASM.org

Outer Dynein Arm Light Chain 1 Is Essential for Controlling the Ciliary Response to Cyclic AMP in *Paramecium tetraurelia*

Osamu Kutomi,[a] Manabu Hori,[b,c] Masaki Ishida,[d] Takashi Tominaga,[e] Hiroyuki Kamachi,[a] France Koll,[c] Jean Cohen,[c] Norico Yamada,[f]* and Munenori Noguchi[a]

Department of Environmental Biology and Chemistry, Graduate School of Science and Engineering, University of Toyama, Toyama, Japan[a]; Division of Environmental Science and Engineering, Graduate School of Science and Engineering, Yamaguchi University, Yamaguchi, Japan[b]; Centre de Génétique Moléculaire, CNRS, Gif-sur-Yvette, France[c]; School of Science Education, Nara University of Education, Nara, Japan[d]; Department of Neurophysiology, Kagawa School of Pharmaceutical Sciences, Tokushima Bunri University, Kagawa, Japan[e]; and Department of Environmental Biology and Chemistry, Faculty of Science, University of Toyama, Toyama, Japan[f]

The individual role of the outer dynein arm light chains in the molecular mechanisms of ciliary movements in response to second messengers, such as Ca^{2+} and cyclic nucleotides, is unclear. We examined the role of the gene termed the outer dynein arm light chain 1 (LC1) gene of *Paramecium tetraurelia* (*ODAL1*), a homologue of the outer dynein arm LC1 gene of *Chlamydomonas reinhardtii*, in ciliary movements by RNA interference (RNAi) using a feeding method. The *ODAL1*-silenced (*ODAL1*-RNAi) cells swam slowly, and their swimming velocity did not increase in response to membrane-hyperpolarizing stimuli. Ciliary movements on the cortical sheets of *ODAL1*-RNAi cells revealed that the ciliary beat frequency was significantly lower than that of control cells in the presence of ≥1 mM Mg^{2+}-ATP. In addition, the ciliary orientation of *ODAL1*-RNAi cells did not change in response to cyclic AMP (cAMP). A 29-kDa protein phosphorylated in a cAMP-dependent manner in the control cells disappeared in the axoneme of *ODAL1*-RNAi cells. These results indicate that *ODAL1* is essential for controlling the ciliary response by cAMP-dependent phosphorylation.

Eukaryotic cilia and flagella are cell organelles for motility and sensing and have various important roles in biological processes. The locomotor behavior of *Paramecium* depends on ciliary movements. The ciliary movements are controlled by changes in the membrane potential that regulate the intraciliary concentrations of Ca^{2+} and cyclic nucleotides. For example, membrane depolarization in response to a mechanical or chemical stimulus applied to the anterior membrane causes an increase in the intraciliary Ca^{2+} concentration (13), which results in a change in the ciliary orientation toward the anterior direction of the cell (ciliary reversal) and a change in the swimming direction (24). Membrane hyperpolarization in response to a mechanical or chemical stimulus applied to the posterior membrane causes an increase in the intraciliary cyclic AMP (cAMP) concentration (38). This induces an increase in the ciliary beat frequency and changes the ciliary orientation to a more posterior orientation, which causes faster forward swimming (11, 25–30). In addition, cAMP suppresses Ca^{2+}-induced ciliary reversal (11, 25–30). However, the molecular bases of the control mechanism of ciliary movements are unclear.

The outer and inner dynein arms, which are multisubunit complexes attached to the outer surface of the peripheral microtubule doublets, generate forces that cause ciliary and flagellar movements. These multisubunit complexes are composed of one or more catalytic heavy chains (HCs) associated with several intermediate chains (ICs) and light chains (LCs). It has been postulated that certain outer dynein arm LCs are responsible for the regulation of ciliary and flagellar movements. For example, the outer dynein arm of *Chlamydomonas reinhardtii* comprises 3 HCs, 2 ICs, and 11 LCs (19). Among the LCs, LC1 associates directly with the catalytic motor domain of γHC (8, 33, 45). The expression of dominant negative LC1 mutant proteins in wild-type *C. reinhardtii* cells showed significant alterations in the flagellar waveform (33). A *Trypanosoma brucei* outer dynein arm LC1 knockdown mutant created by RNA interference (RNAi) exhibited slow backward propulsion and a reversed flagellar beat (6). In addition, the loss of LC1 induced the destabilization of the outer dynein arms. In the planarian *Schmidtea mediterranea*, a reduction in levels of LC1 by RNAi caused a significant drop in the ciliary beat frequency and abolished the ability of beating cilia to form metachronal waves (36). However, the precise role of LC1 of dynein complexes in the molecular mechanisms of ciliary and flagellar movements is unclear. The control of ciliary and flagellar movements depends on second messengers, such as Ca^{2+} and cyclic nucleotides. Therefore, determining how defects of LC1 affect the regulation of the ciliary and flagellar responses to second messengers is essential to an understanding of the role of the dynein subunits in the molecular mechanisms.

We have shown previously that a cortical sheet, an experimental system that we developed, is a useful tool to analyze the ciliary movements of *Paramecium* (26–29, 31). In addition, the *Paramecium tetraurelia* genome database, a ciliary proteome database, and protocols for genetic engineering by RNAi are available (1–4, 14). Therefore, ciliated *Paramecium* could be a useful model organism to study the role of axonemal proteins in the molecular mechanisms of ciliary movements.

In this study, we focused on a gene termed the outer dynein

Received 31 October 2011 Accepted 2 March 2012
Published ahead of print 16 March 2012
Address correspondence to Munenori Noguchi, noguchi@sci.u-toyama.ac.jp.
* Present address: Department of Natural History Sciences, Graduate School of Science, Hokkaido University, Sapporo, Japan.
Supplemental material for this article may be found at http://ec.asm.org/.

doi:10.1128/EC.05279-11

arm light chain 1 gene of *P. tetraurelia* (*ODAL1*), a homologue of the LC1 gene of *C. reinhardtii*. We analyzed the role of *ODAL1* in ciliary movements by RNAi using a feeding method (14). Our results indicate that the *ODAL1* gene is essential for controlling cAMP-dependent ciliary movement.

MATERIALS AND METHODS

Cell culture. *P. tetraurelia* (stock 7.2B) cells were cultured in a hay infusion bacterized with *Enterobacter aerogenes* and supplemented with 0.8 μg/ml β-sitosterol according to standard procedures (40). The cells were grown to the late logarithmic phase at 25°C.

Gene silencing by RNAi using the feeding method. The open reading frame region of *ODAL1* (GenBank accession no. XM_001446309) was amplified by PCR and cloned into the Litmus28i vector (New England BioLabs) between two T7 promoters. The amplification primers used were f1 (ATGGCAAAGACAACTTGTG) and r1 (TCATTTGACAGTGG TTGTAG). The resulting constructs were used for the transformation of HT115, an RNase III-deficient strain of *Escherichia coli* with an isopropyl-β-D-thiogalactopyranoside (IPTG)-inducible T7 polymerase (42). RNAi gene silencing was performed according to a feeding method described previously by Galvani and Sperling (14), with modifications. Wild-type paramecia were incubated in a culture medium containing 0.8 μg/ml β-sitosterol, 100 μg/ml ampicillin, and 0.4 mM IPTG. Gene silencing was initiated by the addition of double-stranded RNA-expressing bacteria to the culture medium (14). One day or two days after the induction of gene silencing, the cells were used for the experiments in this study. The phenotypes of *ODAL1*-silenced (*ODAL1*-RNAi) cells were the same after 1 day and 2 days of gene silencing. Nonsilenced *P. tetraurelia* cells were used as the control cells. As a negative control, we used *ND7* silencing, which affects trichocyst exocytosis without altering the *ODAL1* gene or any other cellular function (16, 37). Furthermore, we analyzed the off-target effect of *ODAL1* silencing using the ParameciumDB *P. tetraurelia* genome database (http://paramecium.cgm.cnrs-gif.fr/) (1).

Competitive PCR. One microgram of each poly(A)$^+$ RNA was reverse transcribed by using PrimeScript reverse transcriptase (TaKaRa Bio Inc., Japan). A 2-μl aliquot of cDNA was added to each PCR mixture, which also contained 1.5 units of *Taq* DNA polymerase, 10 mM Tris-HCl (pH 9.0 at room temperature), 50 mM KCl, 0.1% Triton X-100, 2 mM $MgCl_2$, 0.2 μM deoxynucleoside triphosphates (dNTPs), and 0.4 μM each primer described above. The amplification protocol consisted of one cycle at 94°C for 1 min, 54°C for 30 s, and 72°C for 60 s; 24 cycles at 94°C for 20 s, 55°C for 20 s, and 72°C for 30 s; and a final extension step at 72°C for 5 min. To quantitatively compare the PCR products, we determined the exponential phase of amplification by performing amplification for 15, 20, 25, and 30 cycles, using the *ODAL1* primers 5′-CTTTCTTCAAATGCAATAG-3′ (sense) and 5′-CATTTAGGGTCATCTTTC-3′ (antisense). In addition, as an internal control for cDNA quantity and quality, we amplified the gene for beta-actin by using the primers 5′-TTGATTATGAAGAGGAAA TG-3′ (sense) and 5′-TCTGTGGACAATGGTTGG-3′ (antisense). Amplified PCR products were electrophoresed in 2.0% agarose gels and visualized by ethidium bromide staining. To quantify the relative amounts of each PCR product, the ethidium-stained gels were reversed and analyzed by using ImageJ (National Institutes of Health). The ratios of *ODAL1* mRNA to beta-actin mRNA were calculated based on the densities of the PCR products (7, 15, 32, 39).

Assays of swimming behavior. Approximately 50 μl of a cell culture containing 40 to 50 live cells was placed by a micropipette onto a depression slide. Membrane-hyperpolarizing stimulation was performed by the addition of $CaCl_2$ to attain a Ca^{2+} concentration of 2 mM in the cell culture (22). After the addition of $CaCl_2$, the behaviors of individual cells were observed under a VCT-VBITVb digital microscope (Shimadzu, Japan) and recorded for 1 s. A sequential image of the swimming path was prepared from the recorded frames by using Motic Images Plus 2.1S (Shimadzu, Japan). The forward swimming velocity was determined by measuring the length of the swimming path by using ImageJ. Membrane-depolarizing stimulation was performed by the addition of KCl to attain a K^+ concentration of 50 mM in the cell culture. After the addition of KCl, backward swimming was observed by using a VCT-VBITVb digital microscope, and the duration of the backward swimming was determined.

Preparation and reactivation of cortical sheets from live cells. The preparation of cortical sheets from live cells (intact cortical sheets) was performed according to methods described in our previous paper (31), with slight modifications. Concentrated cells were washed by centrifugation with an ice-cold washing medium containing 2 mM EDTA, 50 mM potassium acetate, and 10 mM Tris-maleate buffer (pH 7.0). The loose pellet of cells was resuspended in 1 ml of an ice-cold potassium acetate solution containing 50 mM potassium acetate and 10 mM Tris-maleate buffer (pH 7.0). The cells were pipetted once or twice through a glass pipette with a small inside diameter (approximately 0.15 mm) to tear or nick the cell cortex. This cell suspension was used for the reactivation experiments. A simple perfusion chamber was prepared by placing the sample between a slide and a coverslip. The slide and coverslip were separated by a thin layer of Vaseline applied to two opposite edges of the coverslip. To observe the reactivation of cilia on the sheet of cell cortex, 50 μl of the sample was gently placed onto a glass slide, and a coverslip with Vaseline was placed over the sample. Solutions were then perfused through the narrow opening at one of the edges of the coverslip, while the excess fluid was drained from the opposite end with the aid of small pieces of filter paper. During the first perfusion using a reference potassium acetate solution, some torn cell cortex adhered flat to the glass surface.

Cortical sheets were perfused successively with reactivation solutions. All reactivation solutions contained 50 mM potassium acetate and 10 mM Tris-maleate buffer (pH 7.0) as well as a component(s), such as $MgCl_2$, ATP, and cyclic nucleotide, as noted in Results and the figure legends. The free Ca^{2+} concentration of 2×10^{-6} M and lower in the reactivation solutions was controlled by using Ca-EGTA buffer (34), using 1 mM EGTA; a concentration of $>2 \times 10^{-6}$ M was obtained by the addition of an adequate amount of $CaCl_2$ to a reactivation solution without EGTA. The reactivation of cilia was carried out at 22°C to 25°C. To determine the ciliary beat frequency, the reactivation of cilia on intact cortical sheets was performed in the presence of 5 μM cyclic GMP (cGMP) throughout, because reactivated cilia without cGMP beat in an abnormal manner to some extent (27).

The ciliary orientation was observed in the presence of 30% glycerol to clearly determine the ciliary orientation (26, 28, 29). Intact cortical sheets were demembranated by perfusion with a Triton solution containing 0.05% Triton X-100, 1 mM EGTA, 1 mM $MgCl_2$, 50 mM potassium acetate, and 10 mM Tris-maleate (pH 7.0) for 1 min and then washed by perfusion with the same solution without Triton X-100 to remove Triton X-100. The demembranated cortical sheets were incubated in a glycerol solution containing 30% glycerol, 1 mM EGTA, 1 mM $MgCl_2$, 50 mM potassium acetate, and 10 mM Tris-maleate (pH 7.0) for 5 min. The cilia were reactivated by perfusion with reactivation solutions containing 30% glycerol, 1 mM ATP, 1 mM $MgCl_2$, 50 mM potassium acetate, and 10 mM Tris-maleate (pH 7.0) as well as Ca^{2+} and cAMP, as noted in Results and the figure legends. In the presence of 30% glycerol, the reactivated cilia on the cortical sheets exhibited only a restricted beat with a small amplitude. However, the pointing directions of the cilia changed in response to Ca^{2+} and cAMP reversibly (26, 28, 29).

Observation and recording of reactivated cilia. The reactivated cilia on cortical sheets were observed under a dark-field microscope equipped with a 100-W mercury light source, a heat filter, and a green filter. The ciliary movements were recorded by using an HAS-220 high-speed camera (Ditect, Japan). To determine the ciliary beat frequency, recording was performed at 600 frames per s, and to determine the ciliary direction, recording was performed at 100 frames per s.

Analysis of ciliary movements on cortical sheets. The movements of the reactivated cilia on intact cortical sheets were analyzed by using ImageJ. We analyzed cilia on the left-hand field of the sheet, defining the surface area of the anatomical left-hand side as the left-hand field of the

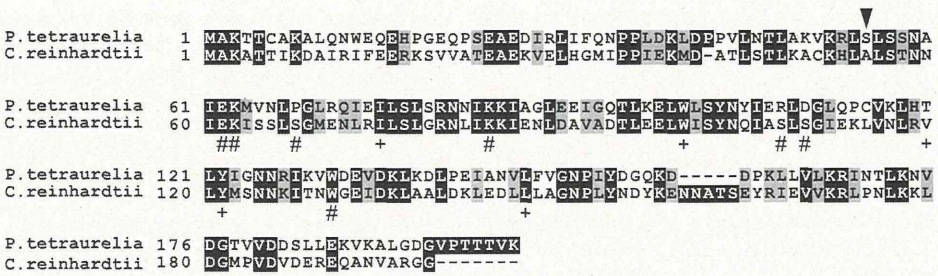

FIG 1 Sequence comparison between *P. tetraurelia* and *C. reinhardtii*. The deduced amino acid sequence alignment between *ODAL1* of *P. tetraurelia* (GenBank accession no. XM_001446309) and the *C. reinhardtii* LC1 gene (accession no. AF112476) was generated with Clustal W (http://www.ebi.ac.uk/Tools/clustalw/) and was displayed by using Boxshade (http://www.ch.embnet.org/software/BOX_form.html). Black boxes indicate identical residues. Gray boxes indicate conservative substitutions. Most of the key residues were conserved, including the γHC catalytic domain binding sites (+) and the tubulin binding sites (#). The arrowhead indicates the putative amino acid (S55), which is strongly predicted to become phosphorylated in a cAMP-dependent manner by the NetPhos 2.0 program (9).

cortical sheets (28). The beat frequency of the reactivated cilia was determined by the direct measurement of the ciliary beat cycle by monitoring the recorded video images frame by frame (31). The method for determining the ciliary orientation was essentially the same as that described in our previous papers (26, 28, 29). Three cilia on several independent cortical sheets from at least two independent RNAi preparations were measured for ciliary beat frequency and ciliary orientation.

Isolation of cilia. Collected cells were washed twice with a washing solution containing 2 mM KCl, 2 mM $CaCl_2$, and 10 mM Tris-maleate (pH 7.0). Cells were deciliated by dibucaine treatment according to methods described previously by Mogami and Takahashi (23), with slight modifications (29). Cilia were isolated from cell bodies by centrifugation twice at 600 × *g* for 5 min. The supernatant was centrifuged at 7,700 × *g* for 10 min to pellet the cilia. The pellet was resuspended in TMKE solution (10 mM Tris-maleate [pH 7.0], 5 mM $MgCl_2$, 20 mM potassium acetate, and 1 mM EGTA) containing 0.3 mM phenylmethylsulfonyl fluoride and centrifuged. The pellet was rewashed with TMKE solution. Each step of the cilium isolation was monitored by dark-field microscopy. Isolated cilia were then treated with a demembranation solution containing 0.1% Triton X-100 in TMKE solution for 10 min at 0°C. The suspension was centrifuged to pellet the axonemes. Triton X-100 was removed from the axonemes by washing twice with TMKE solution. The pellet of the axonemes was suspended in a small amount of TMKE solution.

Phosphorylation of axonemal proteins. The *in vitro* phosphorylation of the axonemes was performed according to methods described previously by Hamasaki et al. (18), with slight modifications. The reaction mixture contained 75 μg axonemes and 30% glycerol in 80 μl TMKE solution as well as test substances. Phosphorylation by endogenous protein kinases was started by the addition of 20 μl of [γ-^{32}P]ATP to attain a final concentration of 2 μM ATP. The ATP concentration of [γ-^{32}P]ATP was 10 μM, and the radioactivity was adjusted to 10 μCi with adenosine 5′-[γ-^{32}P]triphosphate (specific activity, 6,000 Ci/mmol; MP Biomedicals Inc., Solon, OH). Immediately after 10 min of incubation at 0°C, the reaction mixture was centrifuged at 10,000 × *g* for 10 min. The pellet was directly suspended in SDS sample buffer (2% SDS, 5% 2-mercaptoethanol, 10% glycerol, 0.5% bromophenol blue, and 62.5 mM Tris-HCl [pH 6.8]) and incubated at 100°C for 2 min. These SDS-treated samples were then subjected to SDS-PAGE or stored at −20°C for further use. The protein concentration was determined according to methods described previously by Lowry et al. (21), using bovine serum albumin as a standard.

SDS-PAGE and autoradiography. SDS-PAGE was performed by a modification of a procedure described previously by Laemmli (20), using 3-to-15% linear gradient acrylamide gels containing a 0 to 19% glycerol gradient run on a 20- by 16- by 0.1-cm slab gel. The gels were stained with Coomassie blue R-250 for 15 min or with silver (10) and dried on filter paper. Molecular weight standards were obtained from Bio-Rad (Hercules, CA). To produce the autoradiograms, an imaging plate (IP; Fujifilm Corp., Tokyo, Japan) was placed over the dried gels for 2 days. After exposure, the IP was scanned by using a bioimaging analyzer system (BAS-1800; Fujifilm Corp.).

Electron microscopy. For electron microscopy, cells were fixed in 1% (vol/vol) glutaraldehyde in 0.05 M cacodylate buffer (pH 7.2) for 1 h at room temperature. The cells were washed and postfixed in 1% (wt/vol) OsO_4 for 1 h at room temperature. Postfixation was followed by washing in distilled water and then dehydration in a series of increasing concentrations of ethanol and, finally, 100% propylene oxide. The cells were flat embedded in Quetol 812 (Nisshin EM Co., Ltd., Japan). Following evacuation and hardening, the cells were cut out of the block and glued onto another polymerized preshaped block. These cells were serially sectioned in a longitudinal orientation, and all of the sections were picked up on Formvar-supported grids having one large opening. The grids were placed in chronological order so that the exact position of each section within the entire series could be determined. A diamond knife (Nisshin EM Co., Ltd., Tokyo, Japan) and Ultracut E (Reichert, Buffalo, NY) were used for sectioning. Sections were then stained at room temperature with uranyl acetate (43) and lead citrate (35) for 7 min and 3 min, respectively. A transmission electron microscope (H-7000; Hitachi, Tokyo, Japan) operated at 75 kV was used throughout the study.

RESULTS

Characteristics of *ODAL1*. The *ODAL1* gene of *P. tetraurelia* (GenBank accession no. XM_001446309) encodes a protein whose predicted sequence is 38% identical to outer dynein arm LC1 of *C. reinhardtii* (accession no. AF112476), and such a protein was detected in the *P. tetraurelia* genome database and the ciliary proteome database (1–4). The *ODAL1* gene includes the conservation of most residues that directly bind the outer dynein arm γHC catalytic motor domain and tubulin (8, 33, 45) (Fig. 1). It is presumed that the *ODAL1* product has a molecular mass of 22 kDa. The cAMP-dependent phosphorylation site was predicted by using NetPhosK 2.0 (9) (Fig. 1).

Confirmation of *ODAL1* silencing by RNAi. We confirmed the effect of *ODAL1* silencing by RNAi using competitive PCR. *ODAL1* mRNA was expressed over 2-fold compared with beta-actin mRNA in nonsilenced cells (control) (Fig. 2). When the paramecia were fed *E. coli* including a knockdown plasmid, however, the amount of *ODAL1* mRNA was strikingly decreased, even within 1 day after feeding (Fig. 2). Compared to control cells, the level of *ODAL1* mRNA was 6-fold lower in *ODAL1*-silenced paramecia.

Furthermore, the off-target effect of *ODAL1* silencing was analyzed. For *ODAL1* silencing, the RNAi off-target has four genes: 3

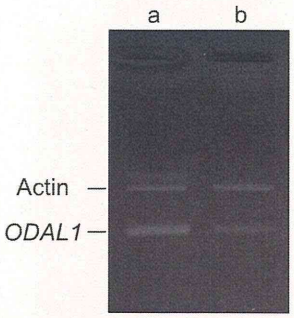

FIG 2 Competitive PCR of *ODAL1*. Shown are electrophoresis images of ethidium bromide-stained gels of *ODAL1* and beta-actin expression in control cells (lane a) and *ODAL1*-RNAi cells (1 day after the induction of gene silencing) (lane b). Each silencing paramecium was grown at 28°C and harvested at 1 day after feeding. One microgram of poly(A)$^+$ RNA of each culture was PCR amplified by using primers specific for the *ODAL1* and beta-actin genes for 25 cycles. Actin and *ODAL1* indicate the PCR products of the beta-actin (loading control) and the *ODAL1* genes, respectively.

genes are itself and its ohnologues, and the other has a completely different function, but its inactivation by this RNAi is very unlikely, since only a single 23-nucleotide (nt) siRNA can target it (data not shown). Therefore, it seems that there are no off-targets and that the RNAi insert is specific.

Phenotypes of *ODAL1*-silenced cells. We examined the phenotypes of *ODAL1*-silenced (*ODAL1*-RNAi) cells. Control cells swam at approximately 0.8 mm/s and showed a significant increase in the forward swimming velocity in response to hyperpolarizing stimulation by the addition of $CaCl_2$ to attain a Ca^{2+} concentration of 2 mM (Fig. 3A and B). In contrast, *ODAL1*-RNAi cells swam at half the swimming velocity of the control cells. Moreover, *ODAL1*-RNAi cells did not show a significant increase in the forward swimming velocity in response to hyperpolarizing stimulation (Fig. 3A and B).

Control cells exhibited backward swimming for approximately 10 s in response to depolarizing stimulation by the addition of KCl to attain a K^+ concentration of 50 mM. In contrast, *ODAL1*-RNAi cells exhibited a long period of backward swimming after the depolarizing stimulation (Fig. 3C). They also exhibited a short period of backward swimming (within 1 s), an "avoiding reaction," frequently seen in culture medium without the depolarizing stimulant (see Movie S1 in the supplemental material). The phenotypes of *ND7*-silenced (*ND7*-RNAi) cells were the same as those of the control cells (data not shown).

Effects of *ODAL1* silencing on ciliary beat frequency in response to Mg^{2+}-ATP. The effects of *ODAL1* silencing on the ciliary beat frequency were determined at various concentrations of Mg^{2+}-ATP by using intact cortical sheets. The ciliary beat frequency of the control cells increased with increasing Mg^{2+}-ATP concentrations up to 8 mM (Fig. 4, and see Movie S2A in the supplemental material). The apparent K_m and V_{max} were 0.80 mM and 52 Hz, respectively. In contrast, the ciliary beat frequency of *ODAL1*-RNAi cells did not increase in the presence of ≥1 mM Mg^{2+}-ATP (Fig. 4, and see Movie S2B in the supplemental material). The apparent K_m and V_{max} of *ODAL1*-RNAi cells (2 days after the induction of gene silencing) were 0.22 mM and 21 Hz, respectively. However, the reactivated cilia of *ODAL1*-RNAi cells showed a normal beat cycle that consisted of an effective stroke and a recovery stroke (37) (see Movie S2B in the supplemental material). The ciliary beat frequency of *ND7*-RNAi cells was essentially the same as that of the control (Fig. 4).

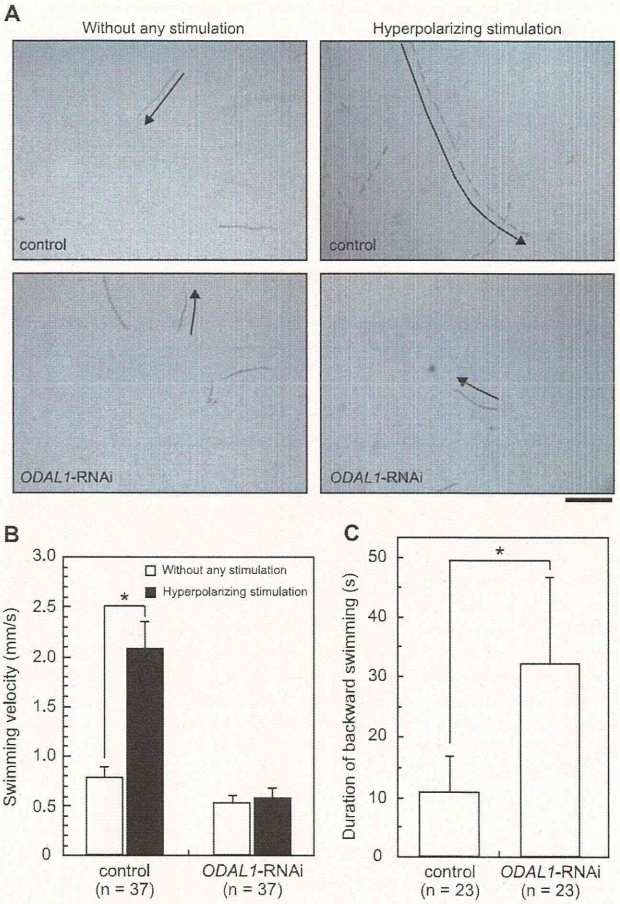

FIG 3 Phenotypes of *ODAL1*-RNAi cells. Swimming behaviors of control cells and *ODAL1*-RNAi cells (2 days after the induction of gene silencing) were observed under certain conditions. Observation and recording were performed as indicated in Materials and Methods. (A) Swimming paths of live paramecia for 1 s without any stimulation and in response to hyperpolarizing stimulation by the addition of $CaCl_2$ to attain a Ca^{2+} concentration of 2 mM. The frame capture rate was 15 frames per s. The arrows indicate the swimming directions. Bar, 0.5 mm. (B) Forward swimming velocity in control cells and *ODAL1*-RNAi cells. In the case of the control, the difference between the swimming velocities under standard conditions and under conditions of hyperpolarizing stimulation was significant (*, $P < 0.01$ by t test). In the case of *ODAL1*-RNAi cells, the difference was not significant. (C) Duration of backward swimming in control and *ODAL1*-RNAi cells. Backward swimming was induced by depolarizing stimulation by the addition of KCl to attain a K^+ concentration of 50 mM. The difference between the durations of backward swimming in control and *ODAL1*-RNAi cells was significant (*, $P < 0.001$ by t test). Boxes and bars indicate means ± standard deviations (SD), respectively. The number of measurements is indicated in each panel (B and C).

Effects of *ODAL1* silencing on ciliary orientation in response to Ca^{2+} and cAMP. The effects of *ODAL1* silencing on the ciliary orientation in response to Ca^{2+} without cAMP were determined by using cortical sheets. The orientation of the reactivated cilia of the control was toward the 6-o'clock position (posterior direction of the cell) at ≤0.2 μM Ca^{2+} (Fig. 5A). When the cortical sheets were perfused with a reactivation solution containing ≥1 μM Ca^{2+}, the orientation of the cilia was toward the 12-o'clock position (anterior direction of the cell) (26, 28, 29). The changes in the

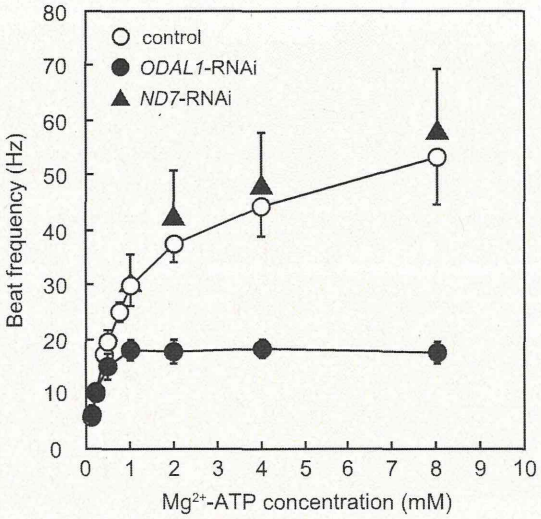

FIG 4 Effect of *ODAL1* silencing on ciliary beat frequency in response to Mg^{2+}-ATP. Changes in the ciliary beat frequency in response to an increasing Mg^{2+}-ATP concentration were determined. Intact cortical sheets from control cells, *ODAL1*-RNAi cells (2 days after the induction of gene silencing), and *ND7*-RNAi cells (2 days after the induction of gene silencing) were perfused successively with reactivation solutions containing 5 μM cGMP, 1 mM EGTA, 50 mM potassium acetate, 10 mM Tris-maleate buffer (pH 7.0), and various concentrations of Mg^{2+}-ATP. The $MgCl_2$ concentration was kept at 1 mM at an ATP concentration of ≤1 mM. The $MgCl_2$ concentration was equal to the ATP concentration at an ATP concentration of >1 mM. Values represent means ± SD (n = 5 to 13).

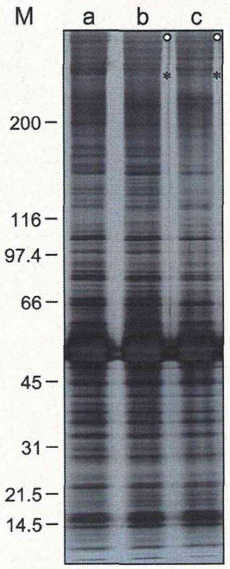

FIG 6 SDS-PAGE patterns of axonemal proteins from *ODAL1*-RNAi cells. The compositions of axonemal proteins from control (lane a), *ODAL1*-RNAi (1 day after the induction of gene silencing) (lane b), and *ODAL1*-RNAi (2 days after the induction of gene silencing) (lane c) cells were analyzed by SDS-PAGE as described in Materials and Methods. Open circles, outer dynein arm HCs; asterisks, an unidentified HC; M, M_r of markers ($\times 10^3$).

ciliary orientation of *ODAL1*-RNAi cells on cortical sheets in response to Ca^{2+} were very similar to those of the control cells (Fig. 5A).

The effects of *ODAL1* silencing on the ciliary orientation on cortical sheets in response to cAMP were determined in the presence of 2 μM Ca^{2+}. In the case of the control cells, the ciliary orientation began to change from an anterior to a posterior direction of the cell in the presence of 1 μM cAMP. At ≥10 μM cAMP, the orientation of the reactivated cilia was toward the 5-o'clock position (posterior direction of the cell). On the contrary, the ciliary orientation of *ODAL1*-RNAi cells did not change from the anterior to the posterior direction of the cell, even in the presence of 100 μM cAMP (Fig. 5B). The ciliary orientation of *ND7*-RNAi cells in response to Ca^{2+} and cAMP was essentially the same as that of control cells (Fig. 5A and B).

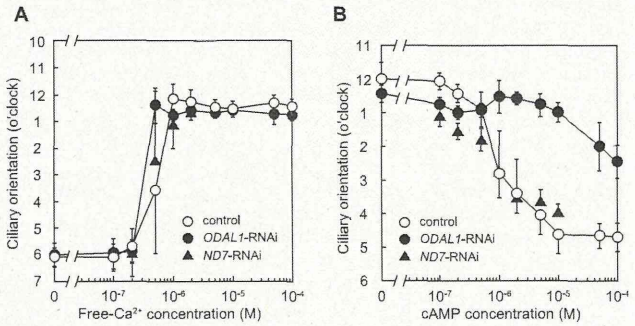

FIG 5 Effects of *ODAL1* silencing on ciliary orientation in response to Ca^{2+} and cAMP. The ciliary orientation in response to Ca^{2+} and cAMP was determined in the presence of 30% glycerol. The demembranated cortical sheets from control, *ODAL1*-RNAi (2 days after the induction of gene silencing), and *ND7*-RNAi (2 days after the induction of gene silencing) cells were perfused successively with reactivation solutions containing 30% glycerol, 1 mM ATP, 1 mM $MgCl_2$, 50 mM potassium acetate, and 10 mM Tris-maleate buffer (pH 7.0) and various concentrations of free Ca^{2+} and cAMP, as noted in the abscissas. The free Ca^{2+} concentration in the reactivation solutions was controlled as indicated in Materials and Methods. The orientation between 11 o'clock and 2 o'clock indicates a Ca^{2+}-induced ciliary reversal. (A) Changes in ciliary orientation in response to Ca^{2+} without cAMP. (B) Changes in ciliary orientation in response to cAMP in the presence of 2 μM Ca^{2+}. Values represent means ± SD (n = 5 to 6).

Change in composition of axonemal proteins after *ODAL1* silencing. The axonemal proteins of *ODAL1*-RNAi cells were analyzed by SDS-PAGE using 3-to-15% polyacrylamide gradient gels. The two HC bands were decreased to some extent in the 1-day- and 2-day-silenced *ODAL1*-RNAi cells (Fig. 6, lanes b and c). The composition of axonemal proteins was not affected by *ND7* silencing (data not shown).

Effects of *ODAL1* silencing on cAMP-dependent phosphorylation of axonemal proteins. We examined the effects of *ODAL1* silencing on the cAMP-dependent phosphorylation of axonemal proteins. In control and the *ND7*-RNAi cells, the 29-kDa and 65-kDa axonemal polypeptides were phosphorylated with 10 μM cAMP (5, 17, 26, 27, 29, 30) (Fig. 7).

In *ODAL1*-RNAi cells, the 65-kDa polypeptide was phosphorylated with 10 μM cAMP, but the phosphorylation of the 29-kDa polypeptide was not detected after 1 day of silencing (Fig. 7A). After 2 days of silencing, no phosphorylation was detected for the 29-kDa or 65-kDa polypeptide (Fig. 7B).

Effects of *ODAL1* silencing on the presence of outer and inner dynein arms within axonemes. Cross sections of cilia from the control, *ODAL1*-RNAi, and *ND7*-RNAi cells were observed by using a transmission electron microscope. In the *ODAL1*-RNAi

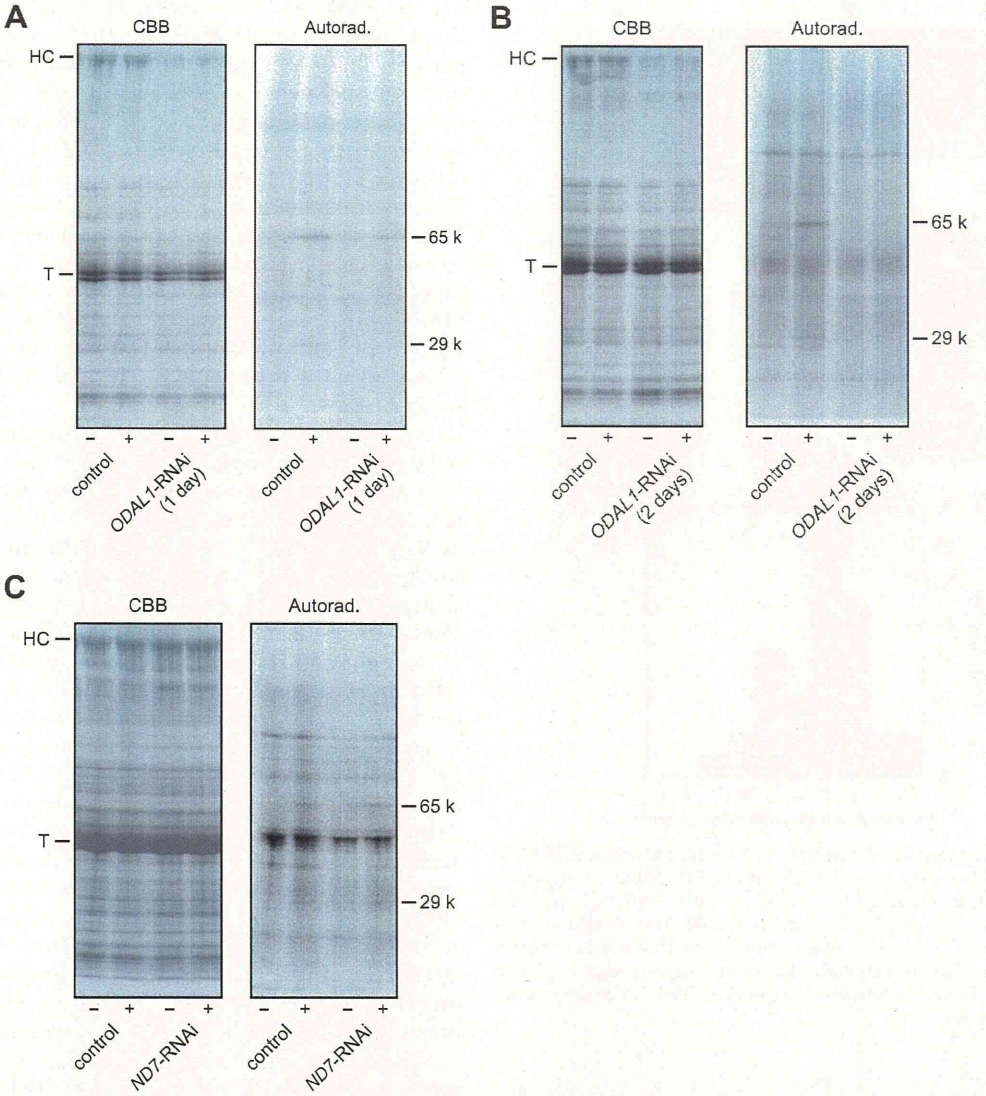

FIG 7 cAMP-dependent phosphorylation of the axonemal proteins from *ODAL1*-RNAi cells. Axonemes were labeled *in vitro* with adenosine 5′-[γ-^{32}P]triphosphate. The phosphorylated proteins were run on 3-to-15% linear gradient acrylamide gels. CBB, band pattern stained with Coomassie blue R 250; Autorad., autoradiogram. (A) Effect of *ODAL1* silencing (1 day after the induction of gene silencing) on the cAMP-dependent phosphorylation of axonemal proteins. (B) Effects of *ODAL1* silencing (2 days after the induction of gene silencing) on the cAMP-dependent phosphorylation of axonemal proteins. (C) Effects of *ND7* silencing on the cAMP-dependent phosphorylation of axonemal proteins. 65 k and 29 k indicate the cAMP-dependent phosphorylated 65-kDa and 29-kDa polypeptides in the autoradiogram, respectively. + and − indicate the presence and absence of 10 μM cAMP, respectively. HC, outer dynein arm HCs; T, tubulins.

axonemes, a couple of the outer dynein arms had disappeared randomly (indicated by arrowheads in Fig. 8A and B). The mean number of missing outer dynein arms was 3.22 ± 1.64 (n = 36) (Fig. 8D). However, the inner dynein arms of *ODAL1*-RNAi were not affected. In the *ND7*-RNAi cells, both the outer and inner dynein arms were not affected (Fig. 8C).

DISCUSSION

Outer dynein arm LC1 has been thought to be responsible for regulating ciliary and flagellar movements. For example, *C. reinhardtii* LC1 binds the outer arm dynein γHC motor domain and a doublet microtubule within the axonemal superstructure and may regulate outer dynein arm activity through a conformational switch for flagellar motility (8, 33, 45). In *T. brucei*, LC1 is necessary for proper forward flagellar motility and for a stable outer dynein arm assembly (6). LC1 of the planarian *S. mediterranea* acts in a mechanosensory feedback mechanism controlling outer arm activity (36). However, the role of outer dynein arm LC1 in the molecular mechanisms of ciliary and flagellar movements is unclear. In this study, we cloned *ODAL1* from *P. tetraurelia* using the *Paramecium* genome database and the ciliary proteome database (1–4). To clarify the role of *ODAL1* in the ciliary movements of *P. tetraurelia*, we created *ODAL1*-silenced cells by RNAi using the feeding method (14) and examined the effects of *ODAL1* silencing on the ciliary movements and the compositions of axonemal proteins. We confirmed that the *ODAL1* gene was properly silenced (Fig. 2) and that *ODAL1* silencing could have no off-target effects. Furthermore, as a negative control, we examined the

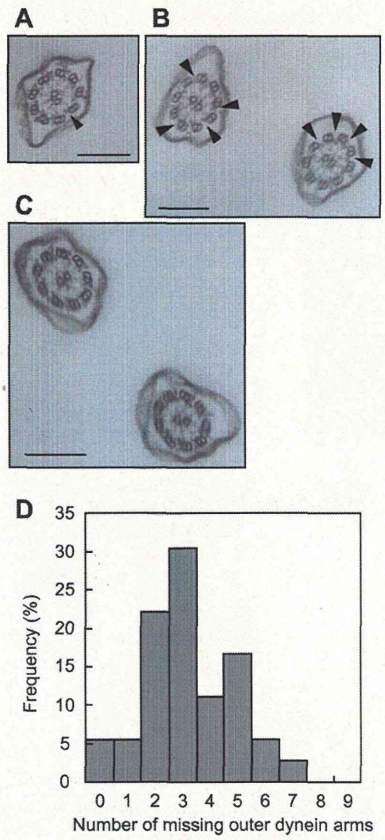

FIG 8 Transmission electron micrographs of cross sections of *ODAL1*-RNAi cilia. Typical cross-sectional images of cilia from *ODAL1*-RNAi (2 days after the induction of gene silencing) (A and B) and *ND7*-RNAi (C) cells were observed by using a transmission electron microscope. The arrowheads indicate the positions of the missing outer dynein arms on the outer doublet microtubules. Bars, 200 nm. (D) Histogram of missing outer dynein arms in *ODAL1*-RNAi axonemes. The abscissa indicates how many outer dynein arms were missing ($n = 36$).

effects of *ND7* silencing, which affects trichocyst exocytosis without altering the *ODAL1* gene or any other cellular function (16, 37). We confirmed that *ND7* silencing did not affect the ciliary movements and the compositions of axonemal proteins (Fig. 4, 5, 7C, and 8C).

We initially examined the phenotypes of *ODAL1*-RNAi cells. They swam more slowly than the control cells, and their swimming velocity did not increase in response to hyperpolarizing stimulation (Fig. 3A and B). In addition, the silenced cells showed a long period of backward swimming in response to depolarizing stimulation and, frequently, a spontaneous avoiding reaction in the absence of depolarizing stimulation (Fig. 3C, and see Movie S1 in the supplemental material). These observations suggest that *ODAL1* silencing resulted in two types of defects in the ciliary activities. The first defect is the impairment of the ability to increase the ciliary beat frequency. The second defect is apparent hypersensitivity to Ca^{2+}.

The ciliary beat frequency depends on the Mg^{2+}-ATP concentration (31) (Fig. 4, and see Movie S2A in the supplemental material). We found that the ciliary beat frequency on intact cortical sheets of *ODAL1*-RNAi cells did not increase with high concentrations of Mg^{2+}-ATP ($\geq$1 mM) (Fig. 4, and see Movie S2B in the supplemental material). This indicates that *ODAL1* silencing impairs the ability to increase the ciliary beat frequency. Therefore, the slow swimming of *ODAL1*-RNAi cells (Fig. 3A and B) is a consequence of the impairment of the ability to increase the ciliary beat frequency. The reactivated cilia of *ODAL1*-RNAi cells showed a normal beat cycle that consisted of an effective stroke and a recovery stroke (41) (see Movie S2B in the supplemental material). This suggests that *ODAL1* silencing does not impair the ciliary waveform. In *C. reinhardtii* and *Tetrahymena thermophila*, an inner dynein arm has been thought to be responsible for the regulation of the ciliary and flagellar waveforms (12, 44). Therefore, the normal ciliary waveform in *ODAL1*-RNAi cells indicates that *ODAL1* silencing does not affect the inner dynein arms of *Paramecium* (Fig. 8).

Previous analyses of ciliary movements using permeabilized cell models (Triton models) and cortical sheets have shown that $\geq$1 μM Ca^{2+} induces a ciliary reversal and backward swimming (11, 24–30). We expected that if *ODAL1*-RNAi cells showed hypersensitivity to Ca^{2+}, the ciliary orientation on cortical sheets would show a ciliary reversal in the presence of lower Ca^{2+} concentrations compared with that of the control cells. However, the threshold Ca^{2+} concentration for the ciliary orientation reversal of the control cells was almost similar to that of *ODAL1*-RNAi cells (Fig. 5A). This indicates that *ODAL1* silencing does not affect sensitivity to Ca^{2+} in the ciliary motor mechanism.

cAMP makes the ciliary orientation more posterior (26, 27, 29). Furthermore, it was shown previously that cAMP and Ca^{2+} act antagonistically in setting the ciliary orientation and that cAMP suppresses Ca^{2+}-induced ciliary reversal (11, 25–30). We analyzed the effect of *ODAL1* silencing on cAMP-dependent ciliary responses using cortical sheets. As shown in Fig. 5B, the ciliary reversal induced by 2 μM Ca^{2+} was not suppressed by cAMP in cortical sheets of *ODAL1*-RNAi cells. This result indicates that *ODAL1* silencing impairs the ciliary response to cAMP. Therefore, the phenotypes of *ODAL1*-RNAi cells, such as the longer period of backward swimming (Fig. 3C) and the spontaneous avoiding reaction in the absence of any stimulation (see Movie S1 in the supplemental material), are probably due to the apparent hypersensitivity to Ca^{2+} that is a consequence of the defect in the ciliary response to cAMP.

To test whether *ODAL1* silencing affects axonemal proteins other than the *ODAL1* product, we analyzed the composition of axonemal proteins in *ODAL1*-RNAi cells using SDS-PAGE. In the axonemes of *ODAL1*-RNAi cells, two HC bands (>200 kDa) were decreased to some extent (Fig. 6, lane b). The upper band corresponds to the outer dynein arm HC (indicated by open circles in Fig. 6). In addition, after 2 days of silencing, several bands of the axonemal proteins also decreased (Fig. 6, lane c). We observed the cross-sectional images of the *ODAL1*-RNAi axonemes with missing outer dynein arms at the level where inner dynein arms were present (Fig. 8). While such defects were rare, we did not see such axoneme cross sections in nonsilenced cells and in *ND7*-RNAi cells. Our observations indicate that as previously shown for *T. brucei* (6), in *P. tetraurelia*, the loss of *ODAL1* also destabilizes the outer dynein arms.

In *Paramecium*, a 29-kDa polypeptide (p29), an LC of the outer dynein arm (22S dynein), is phosphorylated in a cAMP-dependent manner (5, 17, 26, 27, 29, 30) (Fig. 7A and B). The sliding velocity between the outer dynein arm containing p29 and the outer doublet microtubules increased in a cAMP-dependent